Kovove Mater. 58 2020 49–57
DOI: 10.4149/km_2020_1_49

Relationship between microstructure and dry wear behavior of compo-cast nano-$SiC_{(p)}$ + micro-$Gr_{(p)}$/Zn-35Al-1.2Mg-0.2Sr composite under different chilling conditions

S. Liu[1], Q. Yuan[1,2]*, Y. Gong[1], G. Xu[1], W. Qiao[1]

[1] *The State Key Laboratory of Refractories and Metallurgy, Key Laboratory for Ferrous Metallurgy and Resources Utilization of Ministry of Education, Wuhan University of Science and Technology, Wuhan 430081, P. R. China*
[2] *Jiangsu Huaneng Cable Company Limited, Gaoyou 225613, Jiangsu, P. R. China*

Received 6 April 2019, received in revised form 10 July 2019, accepted 9 September 2019

Abstract

In the present experimental research, the compo-casting process was employed to fabricate Zn-35Al-1.2Mg-0.2Sr composite alloy reinforced with nano-$SiC_{(p)}$ + micro-$Gr_{(p)}$ particles and the water-cooling control system casting was applied to realize the effects of different chilling conditions on the as-synthesized material. Also, dry sliding wear experiments were performed to study the wear behavior of Zn-35Al-1.2Mg-0.2Sr composite alloy. Moreover, the effects of nano-$SiC_{(p)}$ + micro-$Gr_{(p)}$ addition on wear behavior of the as-prepared composite at different wear temperatures were analyzed. It was noticed that the abrasive resistance of Zn-35Al--1.2Mg-0.2Sr composite alloy was dependent on the percentage and the dendritic arm spacing of the wearable Al-rich α-phase as well as on the distribution of nano-$SiC_{(p)}$ + micro-$Gr_{(p)}$ particles. With the increase in cooling rate during casting, the dendritic arm spacing of the α-phase decreased apparently. Further, with the increase in wear temperature, the percentage of the wearable Al-rich α-phase, especially for the specimen cooled under a full cooling mode, started to increase significantly. The specimen cooled under a full cooling mode manifested excellent high-temperature abrasive resistance. Furthermore, the tensile strength of the as-cast composite increased with the increase in cooling rate during casting, and it could be attributed to the refined microstructures and the distribution of nano-$SiC_{(p)}$ + micro-$Gr_{(p)}$ particles.

K e y w o r d s: Zn-35Al-1.2Mg-0.2Sr, SiC nanoparticles, Gr microparticles, wear behavior, compo-casting

1. Introduction

Zinc (Zn)-aluminum (Al) alloys have attracted considerable interest in engineering application and material science research due to their excellent mechanical and tribological properties [1, 2]. It is noticeable that energy conservation, environmental protection, and lightweight design are the main topics in current research scenario. Thereupon, multifarious research has been conducted to replace cast iron, lead, and bronze (used for bearings and bushes) with Zn-Al alloys [3–5]. The Al content in Zn-Al alloys is a very important factor, and a small amount of magnesium (Mg) is also beneficial to improve the mechanical properties and the castability of Zn-Al alloys. Yan et al. [6] investigated the effects of Al content (33 to 48 %) on mechanical and wear properties of Zn-based alloys. Abou El-khair et al. [7] found that with an increase in Al content from 8 to 27 %, the mechanical and wear properties of Zn-based alloys increased significantly; a similar outcome was also reported by Prasad et al. [8]. However, it has been observed that the enhanced wear properties of Zn-Al alloys by the addition of Mg, Cu, or other rare-earth elements still do not meet the requirements of transmission drive; therefore, the development of novel Zn-Al alloys with excellent wear properties is imperative. Ceramics are excellent reinforcing materials for metal-matrix composites

*Corresponding author: tel.: +86 15994235997; e-mail address: yuanqing@wust.edu.cn

due to their outstanding physical, mechanical, electrochemical, and wear-resisting properties; therefore, the preparation of Zn-Al alloys with wear-resisting silicon carbide (SiC) particles and friction-resisting graphite (Gr) particles has been sprung up gradually in recent years. Babic et al. [9] revealed that ZA-27 alloys reinforced with Gr particles ($Gr_{(p)}$) yielded significantly lower wear rates and coefficients of friction than the matrix alloy specimens in all combinations of applied loads and sliding speeds during dry and lubricated tests. Mondal et al. [10] used 20–40 μm SiC particles as reinforcement and demonstrated that the wear resistance of the fabricated alloys increased rapidly with the increasing amount of SiC particles (25 to 80 %). To improve the comprehensive performance of matrix alloys, different contents of $SiC_{(p)}$ and $Gr_{(p)}$ particles are often applied to matrix alloys [11, 12]. It was found that the combined effects of $SiC_{(p)}$ and $Gr_{(p)}$ particles on wear properties of Zn-Al alloys were superior to their individual effect. Moreover, the wear properties of Zn-Al alloys could be further improved by microstructure controlling.

The research on the Zn-Al alloys reinforced with $SiC_{(p)}$ and $Gr_{(p)}$ is interesting and worthwhile [13]; however, a very few studies have reported the relationship between dry wear behavior and microstructure of Zn-35Al-1.2Mg-0.2Sr composite alloy reinforced with nano-$SiC_{(p)}$ + micro-$Gr_{(p)}$ particles under different chilling conditions during compo-casting. Hence, the main purpose of the present work was to investigate the dry wear behavior of Zn-35Al-1.2Mg-0.2Sr alloy reinforced with nano-$SiC_{(p)}$ + micro-$Gr_{(p)}$ particles. The relationship between the as-cast microstructure of the alloy and different chilling conditions was clarified. Furthermore, the mechanical properties of Zn-35Al-1.2Mg-0.2Sr alloy under different chilling conditions were analyzed. Also, the effects of nano-$SiC_{(p)}$ + micro-$Gr_{(p)}$ addition on the wear behavior of Zn-35Al-1.2Mg-0.2Sr alloy were discussed. Therefore, the results of the present work could provide useful information for the fabrication of Zn-Al alloy composites.

2. Materials and methods

2.1. Materials preparation

10 wt.% nano-SiC powder particles (purity = 99 wt.%, particle size = 100 nm), 10 wt.% micron-sized Gr powder particles (purity = 99 wt.%, particle size = 2.5 μm), and 80 wt.% pure Al powder (purity = 99.9 wt.%, particle size = 35 μm) were mixed. Moreover, the total weight of the mixed powder was 100 g. Ball-milling was performed in a QM-3SP type laboratory planetary ball mill for 4 h using hardened stainless steel balls (about 10 mm in diameter) immersed in an alcohol solution. The weight ratio of balls and powder and the rotational speed of the ball mill were set to 20 : 1 and 400 rpm, respectively. The parameters of the ball-milling process were adopted from earlier works [14, 15]. Subsequently, the resultant powder mixture and the alcohol solution were separated by filter papers and then dried in a drying oven. The obtained powder was then cold-pressed into an intermediate carrier bulk (in square steel die) at a constant pressure of 100 MPa using a YES-2000 digital hydraulic pressure machine. The pure industrial zinc (99.9 wt.%) and pure aluminum (99.9 wt.%) were then mixed in a graphite crucible and melted at 720 ℃ for 45 min in an electro-resistance furnace. The addition of Mg and Sr were used to accelerate the infiltration process of the nano-$SiC_{(p)}$ + micro-$Gr_{(p)}$. A stainless steel propeller covered by ZnO coating was used to stir the melt at 500 rpm for about 2–3 min in an argon atmosphere. The intermediate carrier bulk was added to the melt, and the stirring was continued for about 10 min until the bulk became completely melted [16, 17].

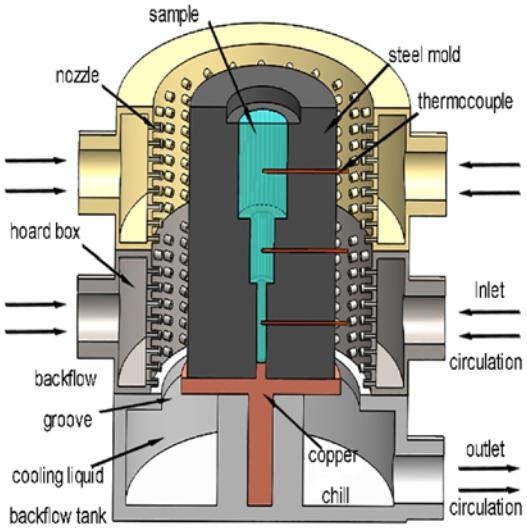

Fig. 1. The equipment of differ-chill mold.

The slagging-off process was conducted after the casting of the melt. Figure 1 displays the equipment with a differ-chill mold for the fabrication of the composite. The total height of the mold was 160 mm. Three cylindrical cavities of diameters 8, 20, and 40 mm were stacked up in a ladder system. Different from conventional controlled directional solidification in the cavity with the same diameter, ladder cavities were designed to obtain a larger discrepancy in the cooling rate. Before casting, the mold was heated to 100 ℃ for several minutes to wipe off the moisture vapor and then placed into the water-cooling control equipment. Also, three k-type thermocouples were installed in the pre-designed positions to monitor the

temperature change during casting in real-time. The water-cooling control equipment operated under full cooling, half cooling, and no cooling modes. The different cooling modes were achieved by the on-off of the hoard box. For the full cooling, all hoard boxes were opened to ensure the complete cooling of the casting liquid, while for the half cooling, only the bottom hoard boxes were applied. For none cooling, all hoard boxes were closed, and the casting liquid was spontaneously cooled.

2.2. Wear test

Dry sliding wear experiments were conducted to analyze the wear behavior of Zn-35Al-1.2Mg-0.2Sr composite alloy. The sliding velocity of the pin-on-disc friction and wear machine was set to 37 $m\,s^{-1}$, and the abrasive disc was fabricated from GCr15 steel with Rockwell hardness (HRC) of 65. The surface of the steel disc was first polished and then cleaned and degreased using water, soap, and ethanol. Moreover, each specimen was ultrasonically cleaned and accurately weighed using a balance (with an accuracy of 0.1 mg) before the wear test. The disc was maintained horizontal, and the pin was mounted vertically on top of the disc along the curved edge. After designing the sliding distance, the test specimen was removed, cleaned with solvents, and weighed to determine the mass loss. The wear rate ($mg\,m^{-1}$) was calculated from the slope of the plot between mass loss and sliding distance after the"running-in" stage (0 to 555 m) [18]. Dry sliding wear experiments were performed at room temperature, and specimen temperatures were measured by a thermocouple inserted perpendicularly to the pin axis at height of 3–10 mm of the contact surface.

2.3. Examination of microstructures and mechanical properties

To reveal the microstructures of wear surfaces, a ZEISS optical microscope was employed. Polished specimens were etched by a solution of 5 g chromium trioxide (CrO_3), 0.5 g sodium sulfate (Na_2SO_4), and 100 mL H_2O. The specimens for optical microscopy were rinsed by a solution of 20 g CrO_3 and 100 mL H_2O. The Vickers hardness of the specimens was measured by a hard meter under a load of 50 gf. The hardness of each specimen was determined by taking an average of 10 hardness acquisitions on the marked points. Also, tensile tests were conducted at room temperature according to ASTM standards using a UTM-4503 electronic universal tensile machine [19]. Repeated tensile tests were performed for each specimen to ensure the accuracy of the measurement.

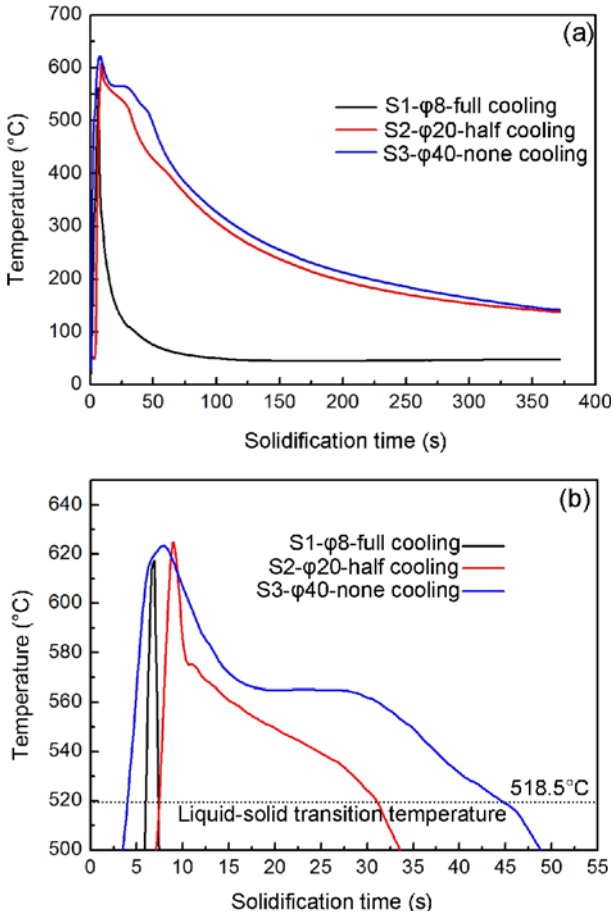

Fig. 2. Transient cooling temperatures with a time of the different cooling castings.

3. Results and discussion

3.1. Microstructures and mechanical properties

Figure 2 reveals the relationship between transient cooling temperature and time for different cooling castings. During the preparation of composite, the temperature of the mixed billet matrix melted in the resistance furnace and the casting temperature were measured as 680 and 625 ℃, respectively. It is observable from Fig. 2b (a local magnification image of Fig. 2a) and the binary phase diagram of Zn and Al that the solid-liquid transition temperature of Zn-35Al-1.2Mg-0.2Sr composite alloy was 518.5 ℃. The cooling rate of the specimen under the full cooling mode (S1) was higher than those under half (S2) and no cooling modes (S3). It took less than 5 s for the S1 specimen to reach the solid-liquid transition temperature, whereas the values were ∼ 22.5 s and ∼ 45 s for the S2 and S3 specimens, respectively.

The microstructures of the as-cast specimens under different chilling conditions are displayed in Fig. 3.

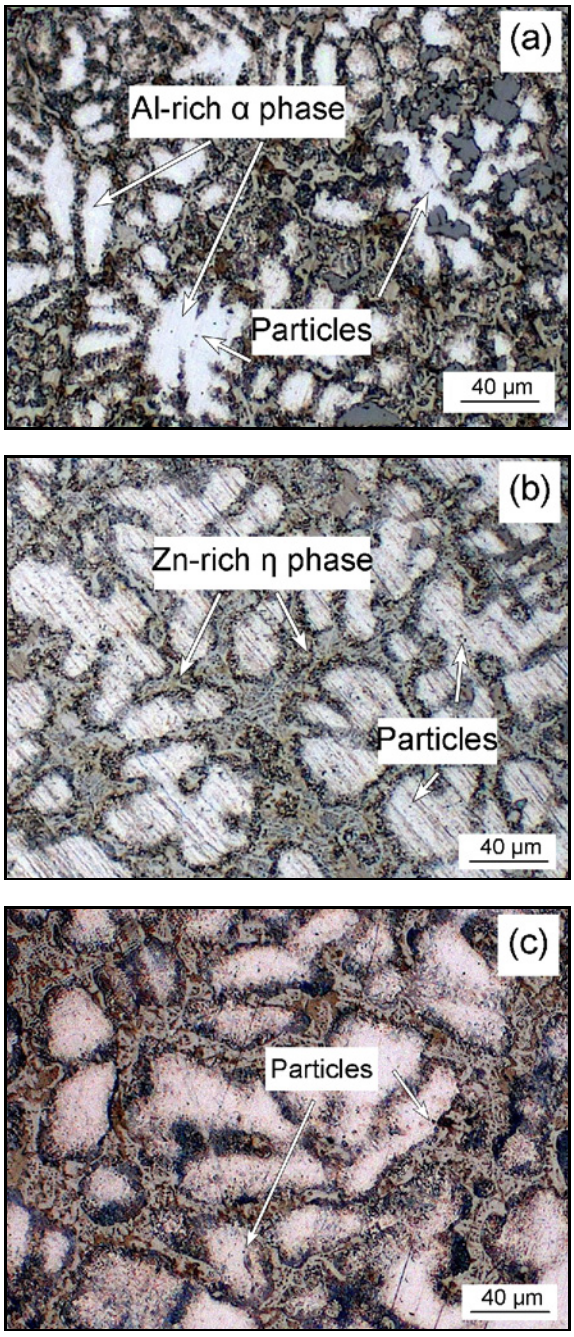

Fig. 3. Microstructures of the as-cast specimens in different chilling conditions: (a) full cooling, (b) half cooling, and (c) none cooling.

It is noticeable that the microstructures of all three specimens were composed of white dendritic Al-rich α-phase, dark Zn-rich η-phase, and nano-$SiC_{(p)}$ + micro-$Gr_{(p)}$. The Al-rich α-phase manifested the properties of a face-centered cubic crystal, and it was the main wear-resisting structure under the heavy load, long-range, and high-speed condition. However, the Zn-rich η-phase was composed of hexagonal crystals, and it was the latent antifriction structure (called as a solid lubricant) for the as-prepared composite alloy. Nano-$SiC_{(p)}$ + micro-$Gr_{(p)}$ were mainly distributed in the α-phase of the S1 and S2 specimens and were located at the boundaries of the α-phase of the S3 specimen. Also, with the decreasing cooling rate, the dimension of the dendritic structure for the Al-rich α-phase became coarse. The morphology difference was caused by different cooling rates during casting. The full cooling mode accelerated the solidification of the α- and the η-phases and hindered the sostenuto growth of these phases.

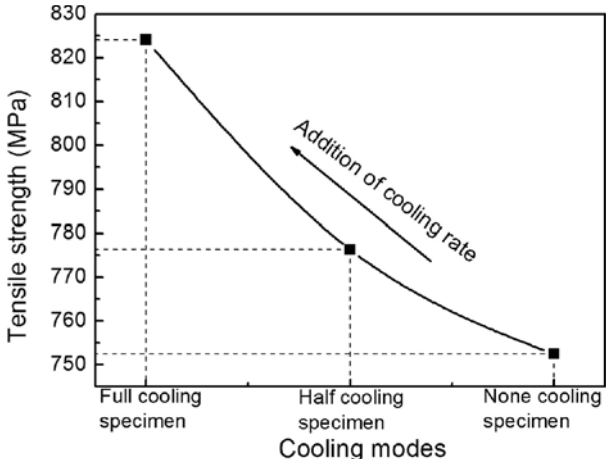

Fig. 4. Tensile strengths of the specimens in different cooling modes.

Figure 4 depicts the tensile strength of the specimens under different cooling modes. It is evident that the values of tensile strength started to decrease from the full cooling mode to the no cooling mode. The S1 specimen yielded the highest tensile strength of 824.0 MPa, whereas the values for the S2 and S3 specimens were measured as $\sim$776.3 and $\sim$752.4 MPa, respectively. Therefore, it can be inferred that the change in tensile strength was closely related to cooling rates of the specimens. During solidification, the liquid composite melt first contacted with the steel mold and the core liquid composite melt then solidified gradually. The effect of nano-$SiC_{(p)}$ and micro-$Gr_{(p)}$ particles (added to the composite melt) on the solidification process was inordinate. When the cooling rate was slow (S3), nano-$SiC_{(p)}$ and micro-$Gr_{(p)}$ particles were pushed aside by the growing grains and then engulfed by grain boundaries, thus they were mainly distributed in the core contraction area in the form of inclusions, which formed innumerable micro-cracks and deteriorated the strength of Zn-35Al-1.2Mg-0.2Sr composite alloy. On contrary, when the cooling rate was fast enough (S1), nano-$SiC_{(p)}$ and micro-$Gr_{(p)}$ particles were not pushed aside by the liquid composite melt, thereby they existed as the second phase in the grain internal, introduced more or less interfacial reactions, and improved the strength of Zn-35Al-

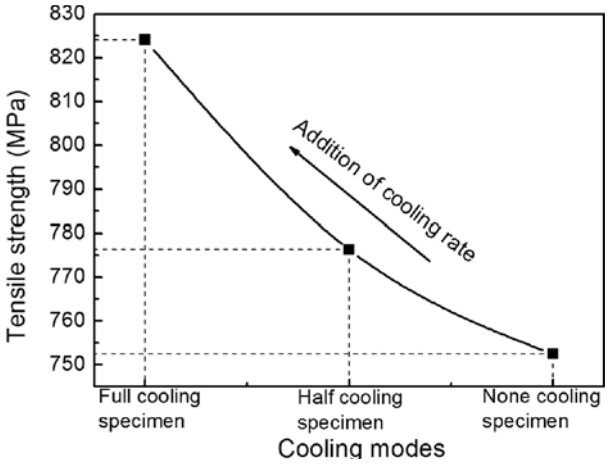

Fig. 5. Wear rate curves with the sliding distance of the three specimens in different cooling modes.

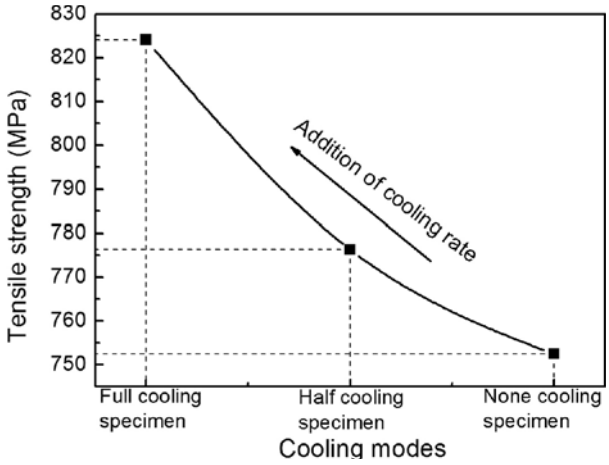

Fig. 6. Relationship between the wear temperature and sliding distance of specimens.

-1.2Mg-0.2Sr composite alloy. Figure 3 presents the distributions of nano-$SiC_{(p)}$ and micro-$Gr_{(p)}$ particles in the specimens under different cooling conditions.

3.2. Wear behavior

Tribological properties, such as friction and wear, are the important performance index for Zn-35Al--1.2Mg-0.2Sr composite alloy. Figure 5 presents the wear rate curves against sliding distance for the specimens under different cooling modes, and a severe disparity was noticed in their abrasive resistance properties. To establish a unified evaluation standard for the wear behavior of Zn-35Al-1.2Mg-0.2Sr composite alloy, abrasion loss in the unit, the sliding distance was used to measure wear rate ($mg\,m^{-1}$). It is obvious from Fig. 5 that the wear rates of all three specimens started to increase with the increasing sliding distance. The wear rate of the S1 specimen was lowest among all three specimens; thus, its wear-resisting behavior was found to be most viable for engineering applications. Also, the wear rate of the S1 specimen increased very slowly and tended to be smooth before and after a sliding distance of 10 km; hence, it indicates that the S1 specimen had an outstanding abrasive resistance with sliding distance. The changes in wear rate for the S2 and S3 specimens were consistent; wear rate increased sharply in the first 1 km and then a relatively slow and an almost linear increase was noticed. However, the wear rate of the S2 specimen was found to be slightly superior to that of the S3 sample. Therefore, the tribological properties of Zn-35Al-1.2Mg-0.2Sr composite alloy were improved significantly with the increased cooling rate during casting.

The relationship between wear temperature and sliding distance for all three specimens is presented in Fig. 6. It is observable that under the same friction condition, the sliding distance of Zn-35Al-1.2Mg-0.2Sr composite alloy increased from 0.824 km (no cooling mode) to 1.895 km (full cooling mode) and the maximum wear temperature decreased from 237 ℃ to 226 ℃. The abrasive resistance of the S1 specimen was nearly double than that of the S3 sample, which can be attributed to the longest sliding distance and the lowest wear temperature of the S1 specimen. Nano-$SiC_{(p)}$ was a hard phase and was composed of space regular tetrahedron structure. Thus its excellent strength and hardness ensured an outstanding abrasive resistance property. Also, during a wear process, the temperature of the wear surface increased rapidly. Due to the remarkable thermal diffusivity and thermal stability of nano-$SiC_{(p)}$, partial energy was transferred quickly, thus resulting in a significant reduction of wear temperature of the wear surface of the S1 specimen. Micro--$Gr_{(p)}$ was a soft phase and was composed of space hexagonal crystal structure. During the wear process, some wear-off micro-$Gr_{(p)}$ particles acted as the solid lubricant on the wear surface between the specimen and the abrasive disc, thus decreased the wear effect and increased the abrasive resistance of the S1 specimen.

To characterize the abrasive resistance properties of the specimens at different wear temperatures, the hardness of the friction contact surface was systematically measured. During the measurement, circles of the same radius were applied to obtain multiple hardness values along the radial direction. Moreover, wear temperatures were controlled by the proceeding of the sliding distance. At the beginning of the wear test, wear temperature was measured as 20 ℃. With the increasing sliding distance, the temperature of the friction contact surface increased rapidly from 20 to 100, 160, and 230 ℃. The distributions of the hardness of the three specimens at different wear temperatures are displayed in Fig. 7. The hardness of the friction contact surface varied profoundly at different wear

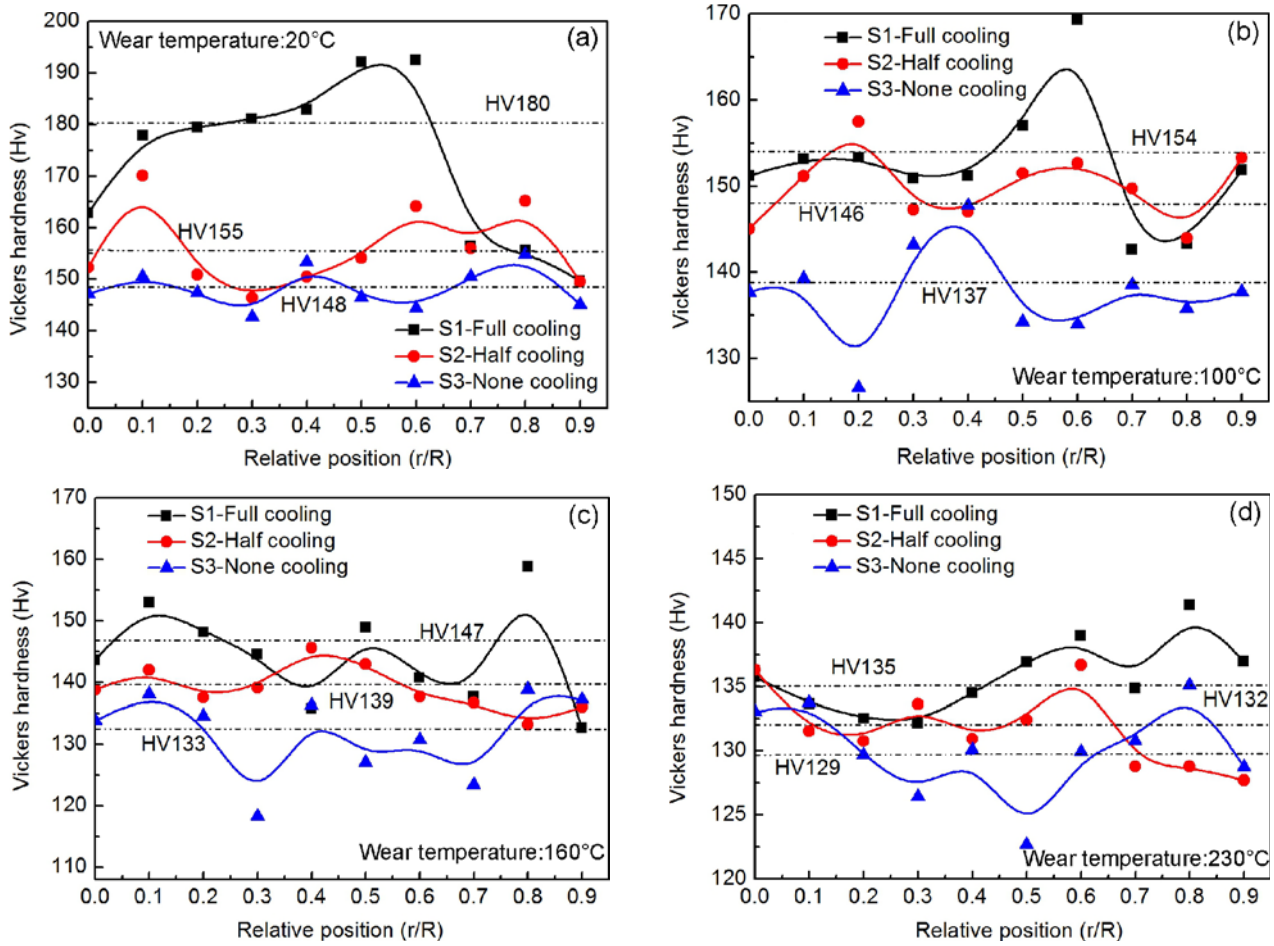

Fig. 7. Microhardness of the friction contact surface at different friction temperatures: (a) 20 °C, (b) 100 °C, (c) 160 °C, and (d) 230 °C.

temperatures. When the wear temperature at the initial wear stage was 20 °C, representing an initial wear stage, the mean micro-hardness of the S1, S2, and S3 specimens reached 180 HV, 155 HV, and 148 HV, respectively. When the wear temperature increased to 100 °C, the values decreased to 154 HV, 146 HV, and 137 HV, respectively. With the increase in wear temperature, the values of mean micro-hardness continued to decrease. Therefore, it can be inferred that the mean micro-hardness of the S1 specimen was higher than those of the S2 and the S3 samples. It also reflects that as compared to the S2 and the S3 samples, the S1 specimen manifested an outstanding abrasive resistance at higher wear temperatures. Furthermore, with the increase in wear temperature, the differences in mean micro-hardness among the specimens were gradually diminished.

Figure 8 exhibits the wear morphologies of the specimens under different cooling modes. An apparent difference was noticed in wear morphologies of the specimens. The wear morphology of the S1 specimen was relatively vague; hence, no prominent scratches were found. Also, bright and dark peeled debris appeared alternately in the microstructure of the S1 sample. In the case of the S3 specimen, long grinding marks, furrows, and scratches were observed on the wear surface. The wear morphology of the S2 specimen lies between those of the S1 and S3 samples. Some relatively vague wear area, scratches, and furrows existed on the wear surface of the S2 sample; however, its scratches and furrows were inconspicuous as compared to those of the S3 sample. The main reason for different wear morphologies can be attributed to the superimposed effects of nano-$SiC_{(p)}$ and micro-$Gr_{(p)}$ particles and as-cast microstructures under different chilling conditions.

The microstructures of the specimens after the wear test are displayed in Fig. 9. As compared to the as-cast morphologies, the three identical phases were noticed in the specimens after the wear test. However, the volume fractions of the Al-rich α-phase and the Zn-rich η-phase, respectively, increased and decreased significantly in all three specimens. It happened because the non-wearable Zn-rich η-phase was easily desquamated after the wear test, and consequently, the wearable Al-rich α-phase was obtained.

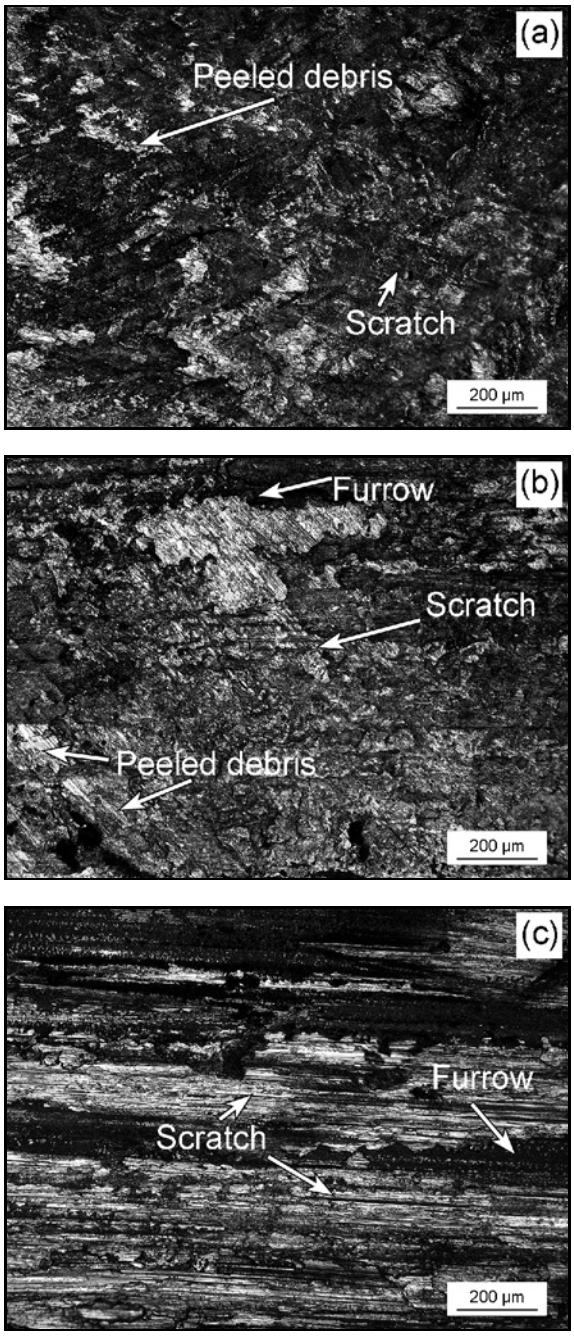

Fig. 8. Wear morphologies of the three specimens in different cooling modes: (a) full cooling, (b) half cooling, and (c) no cooling.

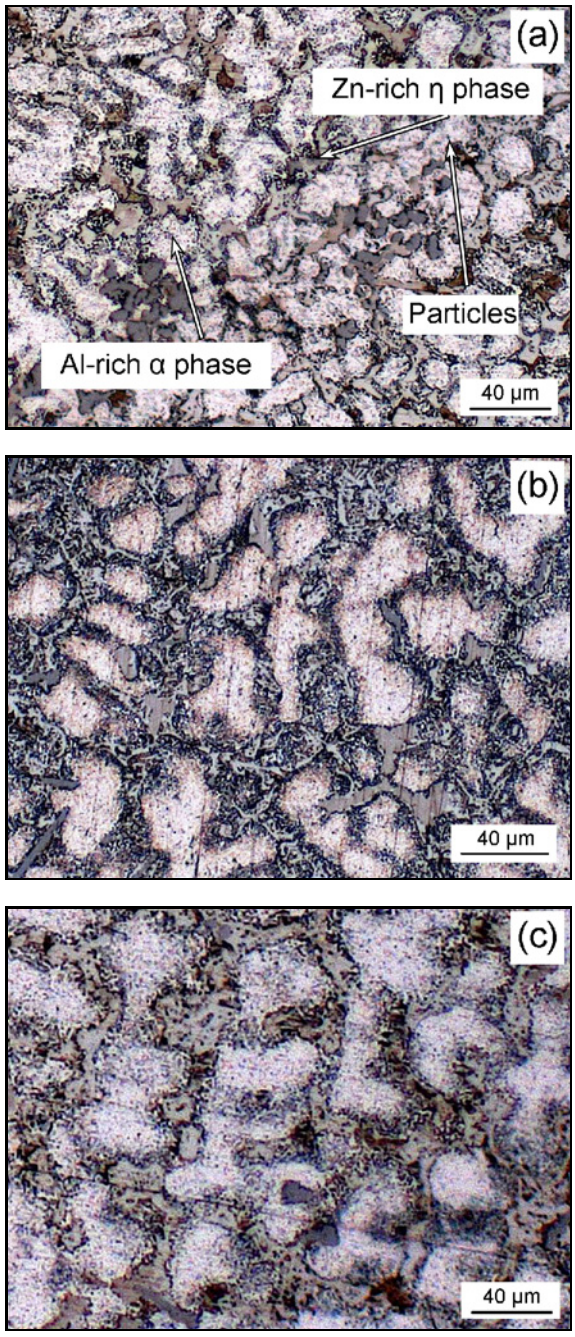

Fig. 9. Microstructures after the wear test of the three specimens in different cooling modes: (a) full cooling, (b) half cooling, and (c) no cooling.

The abrasive resistance property of the Al-rich α-phase was also related to its content and dendritic arm spacing. Figure 10 presents the percentages of the wearable Al-rich α-phase in the specimens at different wear temperatures. Image-Pro Plus, an image processing software, was employed to measure the percentages of the wearable Al-rich α-phase in the samples based on the automatic color difference recognition function [20, 21]. To ensure the accuracy of the measurement, ten images at the same magnification were captured for each specimen [22, 23]. It is detectable from the histogram that the content of the wearable Al-rich α-phase was found to be the largest in the S1 specimen at different wear temperatures except for 20 ℃ and increased significantly with the rise in wear temperature. When the wear temperature was 20 ℃, the amount of the wearable Al-rich α-phase in the S1 specimen was considerably lower than that in the S3

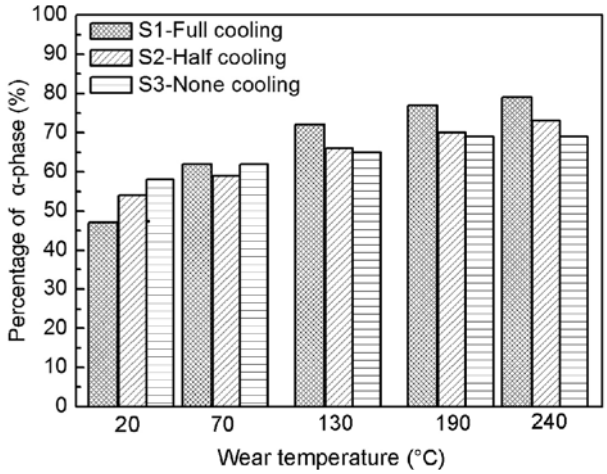

Fig. 10. Percentages of wearable Al-rich α-phase in the three specimens at different wear temperatures.

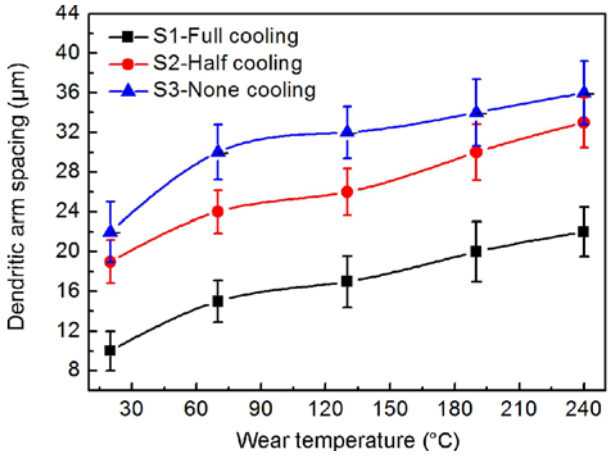

Fig. 11. Measured dendritic arm spacing of α-phase in the three specimens at different wear temperatures.

sample. It happened because the dendritic structure of the Al-rich α-phase was limited to spread at a fast cooling rate. Also, a fast cooling rate led to larger internal stresses between each phase during solidification, thus impeded the growth of the Al-rich α-phase. The increase in the content of the wearable Al-rich α-phase for the S1 specimen was more profound as compared to those of the other two specimens, thus resulting in an excellent abrasive resistance property.

It should be noted that the variations in the contents of the wearable Al-rich α-phase were not consistent with those of the mean micro-hardness. It happened because the dendritic arm spacing of the α-phase at different wear temperatures played a crucial role. Grain refinement caused dislocation stacking and strain hardening. Also, shear strength started to increase with the decrease in dendritic arm spacing of the α-phase under dry sliding friction condition. Thus the abrasive resistance property was significantly improved. Figure 11 presents the measured dendritic arm spacing of the α-phase. To ensure the accuracy of the measurement, about 100 dendritic arm spacings were measured for each specimen based on the chord line method. With the increasing wear temperature, the dendritic arm spacing increased gradually and then became stable. Moreover, the dendritic arm spacing of the S1 specimen was found to be the least among all three specimens, and the S2 and S3 samples yielded almost the same dendritic arm spacing. Therefore, the higher mean micro-hardness of the S1 specimen can be attributed to the duplicate effect of content and dendritic arm spacing of the α-phase.

4. Conclusions

In the present study, Zn-35Al-1.2Mg-0.2Sr composite alloy reinforced with nano-$SiC_{(p)}$ + micro-$Gr_{(p)}$ particles was fabricated by water-cooling control system casting. Dry sliding wear experiments were performed to study the wear behavior of the as-synthesized composite under different chilling conditions. The effects of nano-$SiC_{(p)}$ + micro-$Gr_{(p)}$ addition on wear behavior of the prepared composite at different wear temperatures were analyzed. The main inferences are depicted below.

(1) The abrasive resistance of Zn-35Al-1.2Mg-0.2Sr composite alloy was dependent on content and dendritic arm spacing of the wearable Al-rich α-phase as well as on the distribution of nano-$SiC_{(p)}$ + micro-$Gr_{(p)}$ particles. With the increase in cooling rate during casting, the dendritic arm spacing of the α-phase decreased significantly.

(2) With the increase in wear temperature, the percentage of the wearable Al-rich α-phase increased remarkably, and the specimen cooled under the full cooling mode manifested an excellent high-temperature abrasive resistance property.

(3) Tensile strength increased rapidly with the increase in cooling rate during casting, and it could be attributed to the refined microstructures and the distribution of nano-$SiC_{(p)}$ + micro-$Gr_{(p)}$ particles.

Acknowledgements

The authors gratefully acknowledge the financial support from the National Natural Science Foundation of China (NSFC) (Nos. 51874216 and 51704217), The Open-Fund Innovation Program of The Key Laboratory for Ferrous Metallurgy and Resources Utilization of Ministry of Education (FMRU201305), The Undergraduate Innovation and Entrepreneurship Training Project of Hubei Province (201810488058), and The Special Project of Technological Innovation of Wuhan (2018010402011187).

References

[1] S. Murphy, T. Savaskan, Comparative wear behaviour of Zn-Al-based alloys in an automotive engine application, Wear 98 (1984) 151–161. doi:10.1016/0043-1648(84)90224-2

[2] T. Savaskan, S. Murphy, Mechanical properties and lubricated wear of Zn-25Al-based alloys, Wear 116 (1987) 211–224. doi:10.1016/0043-1648(87)90234-1

[3] H. Çuvalci, H. Bas, Investigation of the tribological properties of silicon containing zinc-aluminum based journal bearings, Tribol. Int. 37 (2004) 433–440. doi:10.1016/j.triboint.2003.10.006

[4] A. Turk, C. Kurnaz, H. Sevik, Comparison of the wear properties of modified ZA-8 alloys and conventional bearing bronze, Mater. Design 28 (2007) 1889–1897. doi:10.1016/j.matdes.2006.04.010

[5] G. Pürcek, T. Savaşkan, T. Kücükőmeroğlu, S. Murphy, Dry sliding friction and wear properties of zinc--based alloys, Wear 252 (2002) 894–901. doi:10.1016/S0043-1648(02)00050-9

[6] Y. Shuqing, X. Jingpe, L. Zhongxia, W. Wenyan, W. Aiqin, L.Jiwen, Influence of Different Al Contents on Microstructure, Tensile and Wear Properties of Zn--based Alloy, J. Mater. Sci. Technol. 26 (2010) 648–652. doi:10.1016/s1005-0302(10)60100-4

[7] M. T. Abou El-khair, A. Daoud, A. Ismail, Effect of different Al contents on the microstructure, tensile and wear properties of Zn-based alloy, Mater. Lett. 58 (2004) 1754–1760. doi:10.1016/j.matlet.2003.10.058

[8] B. K. Prasad, Effects of partially substituting copper by silicon on the physical, mechanical, and wear properties of a Zn-37.5% Al-based alloy, Mater. Charact. 44 (2000) 20050564. doi:10.1016/s1044-5803(99)00057-1

[9] M. Babic, S. Mitrovic, D. Dzunic, B. Jeremic, I. Bobic, Tribological Behavior of Composites Based on ZA-27 Alloy Reinforced with Graphite Particles, Tribol. Int. 37 (2010) 401–410. doi:10.1007/s11249-009-9535-2

[10] D. P. Mondal, S. Das, R. N. Rao, M. Singh, Effect of SiC addition and running-in-wear on the sliding wear behaviour of Al–Zn–Mg aluminium alloy, Mat. Sci. Eng. A 402 (2005) 307–319. doi:10.1016/j.msea.2005.05.023

[11] I. Bobic, J. Ruzic, B. Bobic, M. Babic, A. Vencl, S. Mitrovic, Microstructural characterization and artificial aging of compo-casted hybrid A356/SiC_p/Gr_p composites with graphite macroparticles, Mat. Sci. Eng. A 612 (2014) 7–15. doi:10.1016/j.msea.2014.06.028

[12] T. S. Kiran, M. Prasannakumar, S. Basavarajappa, B. M. Viswanatha, Effect of heat treatment on tribological behavior of zinc aluminum alloy reinforced with graphite and SIC particles for journal bearing, Ind. Lubr. Tribol. 67 (2015) 292–300. doi:10.1108/ilt-08-2013-0090

[13] R. Karslioglu, H. Akbulut, M. Usysal, G. Bagdatli, Tribological behaviours of hybrid Zn-Al metal matrix composites produced by a rapid current sintering technique, Ind. Lubr. Tribol. 66 (2014) 481–489. doi:10.1108/ilt-11-2011-0091

[14] M. R. Rosenberger, A. E. Ares, I. P. Gatti, C. E. Schvezov, Wear resistance of dilute Zn-Al alloys, Wear 268 (2010) 1533–1536. doi:10.1016/j.wear.2010.01.023

[15] R. Mojaver, H. R. Shahverdi, Relationship between cooling rate, microstructure features and wear behavior in end-chill cast Zn-27%Al alloys containing more than 2% Cu, Wear 271 (2011) 2899–2908. doi:10.1016/j.wear.2011.06.014

[16] R. Mojaver, H. R. Shahverdi, The relationship between the wear behavior and microstructure features in end-chill cast Zn-27%Al alloy, Wear 268 (2010) 605–611. doi:10.1016/j.wear.2009.10.007

[17] A. A. El-Daly, M. Abdelhameed, M. Hashish, M. D. Walid, Fabrication of silicon carbide reinforced aluminum matrix nanocomposites and characterization of its mechanical properties using non-destructive technique, Mat. Sci. Eng. A 559 (2013) 384–393. doi:10.1016/j.msea.2012.08.114

[18] W. Hailong, Z. Rui, H. Xing, W. Changan, H. Yong, Characterization of a Powder Metallurgy SiC/Cu-Al Composite, J. Mater. Process. Tech. 97 (2008) 43–48. doi:10.1016/j.jmatprotec.2007.06.002

[19] A. M. Karbalaei, O. Mirzaee, H. R. Baharvandi, Fabrication and study on mechanical properties and fracture behavior of nanometric Al_2O_3 particle-reinforced A356 composites focusing on the parameters of vortex method, Mater. Design 46 (2013) 199–205. doi:10.1016/j.matdes.2012.10.008

[20] A. M. Karbalaei, H. R. Baharvandi, O. Mirzaee, Nano-sized aluminum oxide reinforced commercial casting A356 alloy matrix: Evaluation of hardness, wear resistance and compressive strength focusing on particle distribution in aluminum matrix, Composites: Part B 52 (2013) 262–268. doi:10.1016/j.compositesb.2013.04.038

[21] A. E. Ares, C. E. Schvezov, Influence of Solidification Thermal Parameters on the Columnar-to-Equiaxed Transition of Aluminum-Zinc and Zinc-Aluminum Alloys, Metall. Mater. Trans. A 38 (2007) 1485–1499. doi:10.1007/s11661-007-9111-z

[22] M. Turhal, T. Savaskan, Relationships between secondary dendrite arm spacing and mechanical properties of Zn-40Al-Cu alloys, J. Mater. Sci. 38 (2003) 2639–2646. doi:10.1023/A:1024434602540

[23] T. Savaşkan, A. P. Hekimoğlu, G. Pürçek, Effect of copper content on the mechanical and sliding wear properties of monotectoid-based zinc-aluminium-copper alloys, Tribol. Int. 37 (2004) 45–50. doi:10.1016/S0301-679X(03)00113-0

[24] A. K. P. Rao, K. Das, B. S. Murty, M. Chakraborty, Microstructural and wear behavior of hypoeutectic Al-Si alloy (LM25) grain refined and modified with Al-Ti-C-Sr master alloy, Wear 261 (2006) 133–139. doi:10.1016/j.wear.2005.09.012

[25] A. K. P. Rao, K. Das, B. S. Murty, Microstructure and the wear mechanism of grain-refined aluminum during dry sliding against steel disc, Wear 264 (2008) 638–647. doi:10.1016/j.wear.2007.05.010

[26] K. G. Basavakumar, P. G. Mukunda, Influence of Grain Refinement and Modification on Dry Sliding Wear Behaviour of Al-7Si and Al-7Si-2.5Cu Cast Alloys, J. Mater. Process. Tech. 186 (2007) 236–245. doi:10.1016/j.jmatprotec.2006.12.039

[27] J. Campbell, Casting, Oxford, Butterworth-Heine--mann, 2003. ISBN 9780080488448